



g-C₃N₄/TiO₂ nanocomposite coated with zinc oxide for selective photocatalytic degradation of nitrate in aquatic media

Mohammad Hadi Ghasemi¹, Reyhaneh Kaveh^{2,a)} , Hassan Alijani³, Elham Asadi⁴, Elaheh Bohloulbandi¹, Majid Baghdad⁵

¹ Applied Chemistry Research Group, ACECR-Tehran Organization, Tehran, Iran

² Department of Inorganic Chemistry, Faculty of Chemistry, Kharazmi University, Tehran 15719-14911, Iran

³ Department of Chemistry, Faculty of Science, Shahid Chamran University of Ahvaz, Ahvaz, Iran

⁴ Faculty of Chemistry, Shahrood University of Technology, Shahrood, Iran

⁵ School of Environment, College of Engineering, University of Tehran, Tehran, Iran

^{a)} Address all correspondence to this author. e-mail: reyhanehkaveh@khu.ac.ir

Received: 17 July 2023; accepted: 12 January 2024; published online: 12 February 2024

Healthy drinking water, free of toxic chemicals, is essential for human health. Nitrate ion in water causes poisoning. Photocatalytic removal of nitrate from water and its conversion to nitrogen gas is of great importance. Heterogeneous photocatalytic nanocomposite g-C₃N₄/TiO₂/ZnO (CTZ) has been considered in this study to remove nitrate in the presence of UV light and formic acid as hole scavenger. The CTZ structure was characterized using FT-IR, SEM, EDS, TEM, BET, and XRD techniques. In this work, an aqueous solution containing NO₃⁻-N anion (50 mg L⁻¹) was examined using different CTZ. Nitrate removal results showed the highest rate 95.24% in the first 60 min. The use of CTZ was associated with improved results in nitrate reduction under visible light irradiation (91.82% nitrate conversion, 95.39% N₂ selectivity). Promising results under visible light are attributed to decrease in the CTZ bandgap, and thus the ease of electron-hole pair formation.

Introduction

Environmental pollution, which is caused by the lack of importance of humans in releasing waste water in nature, is a global problem that threatens human life and the future of the planet. Therefore, the control of the discharge process and how to remove pollutants should be considered [1–4]. The use of efficient and inexpensive photocatalysts with high production capability is one of the new solutions that results in the highest conversion and reduction of pollutants with the least waste. The significant progress of photocatalysts in environmental purification in the last few years shows the importance of using these composites. Multi-component composites such as Cd_{0.5}Zn_{0.5}S/Bi₂MoO₆ in oxytetracycline degradation [5], MIL-101(Fe)/BiOBr in the photocatalytic reduction of Cr(VI) and enrofloxacin [6], Ta₃N₅/CdS in the photocatalytic removal of tetracycline and Cr(VI) [7], TCPP/Bi₁₂O₁₇C₁₂ for boosting photodegradation of tetracycline hydrochloride [8], UTSA-16 in the CH₄ and CO₂ adsorption [9], TaON/Bi₂WO nanofibers for

efficient abatement of antibiotics and Cr(VI) [10] and Bi₂WO₆/C₃N₄/carbon fiber cloth composite photocatalyst for efficient water decontamination [11] have been reported.

Contamination of nitrates (NO₃⁻) is becoming a significant challenge due to groundwater contamination and human health toxicity such as cancer and the blue-baby disease [12]. The wide use of synthetic fertilizers, poor disposal, and highly stable nitrate content in aqueous solutions enable it widely pervasive [13]. The development of effective nitrate removal methods is an essential request. General techniques for removing nitrate from wastewater, such as catalytic reduction, adsorption, chemical, and biological denitrification, are expensive, difficult to fulfillment and generally require post-treatment of the effluents produced [14–17].

Heterogeneous photocatalysis over semiconductors permits the use of ultra-violet irradiation in different chemical reactions, among which overall water splitting is maybe the most common one owing to the global energy crisis [18]. Numerous research

documents have been published, prompting fast development in this direction. On the other hand, the photocatalytic removal of nitrate ions in an aqueous solution is less studied. The reasons include that it is challenging to find a competent photocatalyst fulfilling both high efficiency and high gases nitrogen selectivity because NO_3^- is soluble and highly stable in aqueous solution. The rather complicity in the mechanism of nitrate reduction [19], compared to water splitting, also contributes to the fewer achievements in this examination field. Among support materials, titanium dioxide relatively enhances pollutant decrease in wastewater due to high surface areas, large pore sizes, and good adsorption ability [20].

As an efficient photocatalyst for environmental decontamination, titanium dioxide surface modification has been extensively studied due to its unique properties such as strong oxidation capability, low cost, and thermal and chemical stability [21–23]. However, its photocatalytic performance is restricted by the rapid recombination of photo-induced pairs of electron-hole and considerable band gap energy (3.2 eV for anatase TiO_2). Much research has been done to improve the photocatalytic performance of TiO_2 , such as deposition of metal or metal oxide [24, 25], doping with nonmetal elements [26], surface sensitization [27], and coupling of composite semiconductor [28], which are useful in promoting the photocatalytic activity of TiO_2 . Recent studies suggest that the unique electronic band structure of graphitic carbon nitride ($\text{g-C}_3\text{N}_4$) can improve composite photocatalytic performance [29]. Because of its tri-s-triazine-based building blocks, the bandgap in the indirect semiconductor graphitic carbon nitride is highly stable under severe thermal and chemical conditions [30]. Previous works have shown that in the $\text{g-C}_3\text{N}_4/\text{TiO}_2$ composite photocatalyst, TiO_2 is covalently bonded to carbon nitride, resulting in higher efficiency photocatalytic reactions [31]. Although recent environmental photocatalysis experiments show a much better photocatalytic efficiency [32–34], the photocatalytic activity of $\text{g-C}_3\text{N}_4/\text{TiO}_2$ in nitrate removal from wastewater is still unclear, and more modification on this composite is needed.

Following our previous research on environmental remediation [35, 37], we investigated the synergistic effects of Zinc Oxide (ZnO) nanoparticles, graphitic carbon nitride, and TiO_2 on the photocatalytic reduction of nitrate. Although the ternary nanocomposite $\text{g-C}_3\text{N}_4/\text{TiO}_2/\text{ZnO}$ has already been developed in a different way, it has been used for photocatalytic degradation of p-toluenesulfonic acid (p-TSA) under visible light [38]. In this research, the ternary nanocomposite $\text{g-C}_3\text{N}_4/\text{TiO}_2/\text{ZnO}$ was prepared in a different way that makes it cost-effective to produce at higher scales. In fact, the pure ZnO nanoparticles, graphitic carbon nitride, $\text{g-C}_3\text{N}_4/\text{TiO}_2$ nanocomposite, and finally, the ternary nanocomposite $\text{g-C}_3\text{N}_4/\text{TiO}_2/\text{ZnO}$ were synthesized and the structure of these compounds was then carefully characterized. Finally, the photocatalytic effects of the

mentioned substances individually on the degradation of aqueous nitrate under UV-visible irradiation was investigated. Due to the Vander Waals force and the coordination interaction between the metal ions and the $-\text{NH}_2$ functional groups in $\text{g-C}_3\text{N}_4$, Zn^{2+} ions were adsorbed into the surfaces $\text{g-C}_3\text{N}_4/\text{TiO}_2$ layers. The nuclei of the $\text{Zn}(\text{HCO}_3)_2$ were formed by the addition of NH_4HCO_3 and gradually grew at increased temperatures on $\text{g-C}_3\text{N}_4$ layers. Finally, the product was produced at a high temperature under N_2 flow. This research was innovative in terms of using the ternary nanocomposite $\text{g-C}_3\text{N}_4/\text{TiO}_2/\text{ZnO}$ in the removal of aqueous nitrate.

Results and discussion

Photocatalyst characterization

The FT-IR analysis of ZnO, TiO_2 , $\text{g-C}_3\text{N}_4$ and CTZ samples were shown in Fig. 1. In the FT-IR spectrum of ZnO, a significant vibration at about 500 cm^{-1} was related to the characteristic stretching of Zn–O bond. Also, a broad peak ranging from 3000 to 3500 cm^{-1} (stretching) as well as 1300 to 1660 cm^{-1} (bending) showed the presence of hydroxyl residue that is because of the atmospheric moisture [39, 40]. FT-IR spectrum of TiO_2 showed a peak ranging from 400 to 700 cm^{-1} which could be related to Ti–O–Ti stretching vibration and a board peak at 3400 cm^{-1} was attributed to $-\text{OH}$ stretching vibration [41]. In the FT-IR spectrum of $\text{g-C}_3\text{N}_4$ attributed to the stretching and rotational vibration of C–N and C–NH bonds. The broad peak at 2900 – 3600 cm^{-1} could be related to stretching modes of the NH group. Also, a sharp peak at 808 cm^{-1} was related to the breathing mode of the s-triazine ring system in the $\text{g-C}_3\text{N}_4$ [42]. The FT-IR spectrum of the CTZ composites exhibited all the main characteristic peaks of ZnO, TiO_2 , and $\text{g-C}_3\text{N}_4$ indicating the presence of aforementioned compounds in the CTZ composites.

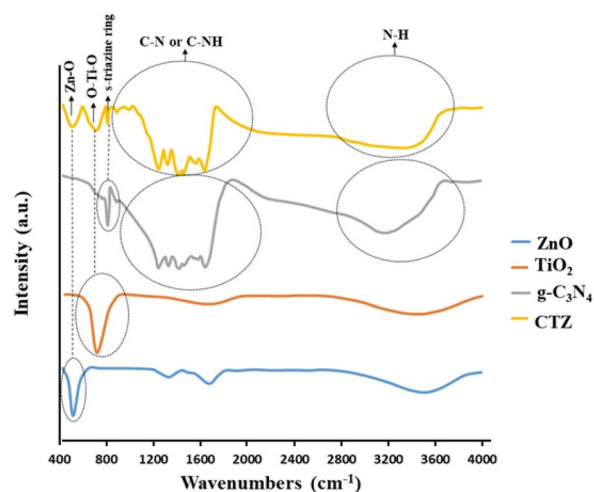


Figure 1: FT-IR Analysis of ZnO, TiO_2 , $\text{g-C}_3\text{N}_4$, and CTZ.

The SEM images of TiO_2 , $\text{g-C}_3\text{N}_4$, and CTZ were shown in Fig. 2. It vividly depicted that TiO_2 nanoparticles were agglomerated and almost spherical in shape (Fig. 2(a)). The SEM of

pure $\text{g-C}_3\text{N}_4$ in Fig. 2(b) showed a plate-like bulk structure. As observed in Fig. 2(c), the nanoparticles of TiO_2 and ZnO are supported on the $\text{g-C}_3\text{N}_4$ surfaces. From Fig. 2(c), it was

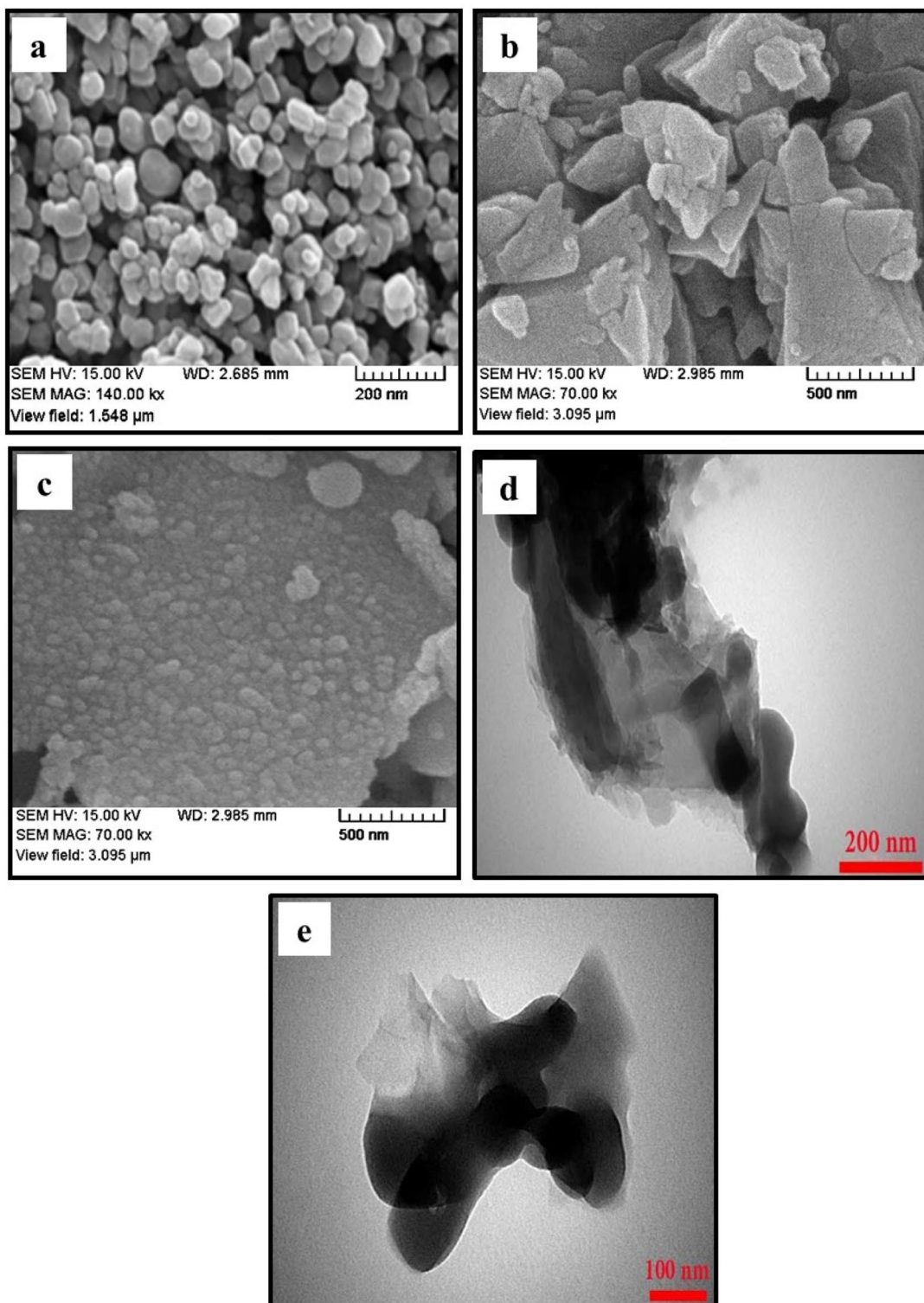


Figure 2: SEM images of (a) TiO_2 , (b) $\text{g-C}_3\text{N}_4$, (c) CTZ, (d) and (e) TEM images of CTZ.

clearly observed the formation of g-C₃N₄ nanoplatelets incorporated TiO₂ and ZnO nanoparticles. Transmission Electron Microscope (TEM) images of CTZ are indicated in Fig. 2(d) and e. As shown, the bulk g-C₃N₄ was etched as a crumpled coated sheet-like structure. The morphology of nanophotocatalyst CTZ was similar to g-C₃N₄ morphology, implying that TiO₂ and ZnO nanoparticles were dispersed on the special graphitic-like structure [43].

The g-C₃N₄/TiO₂ and CTZ nanocomposites were analyzed with EDS, and the results were collected in Table S1. The atomic percentage of CTZ nanocomposite, including carbon, nitrogen, oxygen, titanium, and zinc, was 11.45, 5.11, 42.05, 23.36, and 18.03%, respectively. The presence of zinc (34.11% by Weight) in the CTZ nanocomposite showed that zinc oxide was properly fixed on the outer layers of the g-C₃N₄/TiO₂ nanocomposite.

The crystalline phases of series composites were represented by XRD patterns. The X-ray diffraction (XRD) analysis of ZnO, TiO₂, g-C₃N₄, g-C₃N₄/TiO₂, and CTZ were indicated in Fig. 3. X-ray diffraction peaks confirmed that ZnO with wurtzite phase (JCPDS: 36-1451) and TiO₂ with anatase phase agreed with the reported JCPDS data (21-1272) and no characteristic peaks were observed other than ZnO and TiO₂ in both ZnO and TiO₂ samples, respectively. Also, the XRD diffraction pattern of g-C₃N₄ showed a broad peak at the 2θ value of 27.5°, related to (002) planes that completely matched with JCPDS data (87-1526) for g-C₃N₄. The peaks for pure ZnO, TiO₂, and g-C₃N₄, were matched well with the corresponding peaks in the CTZ pattern. Characteristic peaks without observable position changes in pure TiO₂, pure ZnO, pure g-C₃N₄, g-C₃N₄/TiO₂, and CTZ, indicating that the crystal

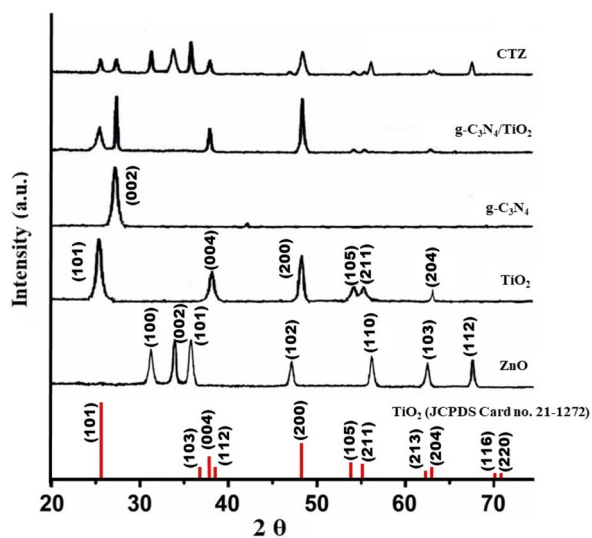


Figure 3: XRD patterns of ZnO, TiO₂, g-C₃N₄, g-C₃N₄/TiO₂, and CTZ.

type of bulk g-C₃N₄ may not be destroyed by chemical modification [44–48].

Nitrogen adsorption–desorption isotherms of g-C₃N₄, TiO₂, ZnO, g-C₃N₄/TiO₂, and CTZ at 77K were measured (Table S2). Surface areas were determined by BET method and average pore size distributions were calculated by BJH method. The surface area and pore volume of CTZ was enlarged significantly compared with pure g-C₃N₄, pure TiO₂, and pure ZnO, which provided improved adsorptivity for CTZ.

To investigate the optical properties of prepared samples, the UV–vis diffuse reflectance spectra (DRS) were used. The TiO₂ spectrum was also carried out as a comparison (Fig. 4). The absorption edge of TiO₂ is below 390 nm, which can only respond to UV light. At wavelengths longer than 400 nm, all composites show an increased absorption compared to the absorption edge of pure TiO₂. g-C₃N₄ and TiO₂/g-C₃N₄ spectra showed the absorption sharp edges around 400 nm. The TiO₂/g-C₃N₄ nanocomposite exhibited increased absorption in the visible light region compared to pure TiO₂ due to the creation of the heterojunction of TiO₂ and g-C₃N₄. This suggested strong visible light photocatalytic activity for TiO₂/g-C₃N₄. Fig. S1 showed the bandgap values of TiO₂, g-C₃N₄, g-C₃N₄/TiO₂, and CTZ, which were calculated by extrapolating the linear portion of (Ahv)² versus photon-energy plots at (Ahv)² = 0. In the TiO₂/g-C₃N₄ and CTZ composites, the bandgap was lower than TiO₂ and g-C₃N₄ (Table S3), which facilitated the generation of photo-generated charge carriers under visible light illumination [49, 50].

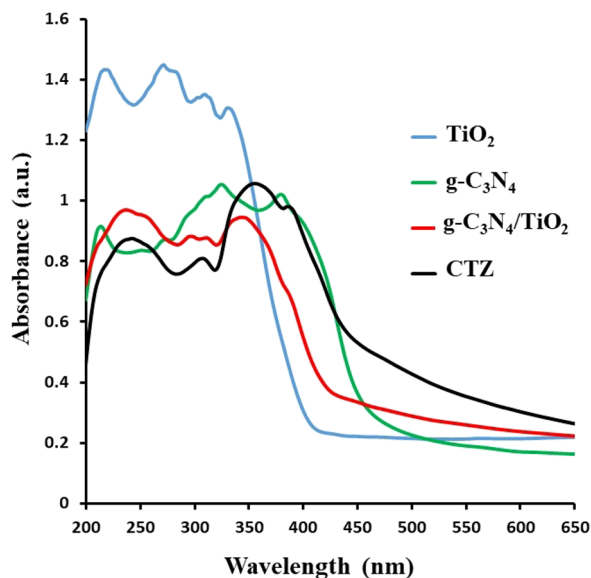


Figure 4: UV–vis DRS spectra of g-C₃N₄, TiO₂, and TiO₂/g-C₃N₄, and CTZ photocatalyst.

Evaluation of photocatalysts performance

Three forms of products, nitrite, ammonia, and nitrogen gas, are produced during the photocatalytic reduction reaction. Nitrogen gas is the most desirable product, ensuring complete nitrate reduction. According to the literature, formic acid is used as the hole scavenger for photocatalytic investigation because of the higher nitrate conversion [36]. Before light irradiation, the aqueous nitrate solution (50 mg L⁻¹) containing the various photocatalysts (50 mg) was stirred in the dark for 1 h to determine the adsorption rate of the catalyst to study the non-photocatalytic removal. After reaching the equilibrium adsorption state (in the dark condition), the amount of the pollutant adsorbed onto pure ZnO, TiO₂, g-C₃N₄, g-C₃N₄/TiO₂, and CTZ was approximately calculated to be 4.3%, 7.1%, 3.6%, 7.4%, and 8.6% of the initial amount of pollutant, respectively. Consequently, the removal of pollutant in dark condition could be neglected. In the dark, no electron-hole pairs can be formed and photocatalytic behaviour of the prepared samples is not induced. The performance of various synthesized catalysts was measured with varying reaction times. The performance data for the photocatalysts according to the selectivity and nitrate conversion efficiency under UV irradiation are shown in Table 1. The photocatalytic system using CTZ exhibited an improved conversion of nitrate compared to other photocatalysts (Table 1; Fig. 5). It highlights the impact of the ZnO layer in the CTZ photocatalyst for improved conversion of nitrate and the increased selectivity to N₂. In conclusion, the CTZ as photocatalyst has the highest rate of conversion of nitrate to nitrogen gas in the presence of formic acid (Table 1, Entry 5). Increasing the irradiation time to 120 min did not significantly affect the nitrate reduction efficiency (Table 1, Entry 6). In the absence

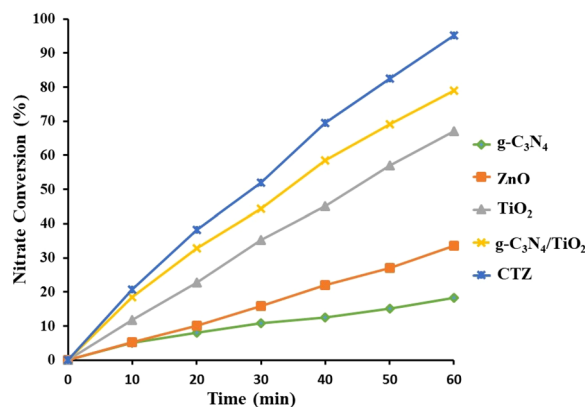


Figure 5: Nitrate reduction using different photocatalysts: ZnO, TiO₂, g-C₃N₄, g-C₃N₄/TiO₂, and CTZ.

of formic acid as a hole scavenger, the photocatalyst would not affect reducing nitrate (Table 1, Entry 7).

The N₂ selectivity for the ZnO, TiO₂, g-C₃N₄, g-C₃N₄/TiO₂, and CTZ photocatalysts in the photoreduction of aqueous nitrate were shown in Fig. 6. The CTZ photocatalyst was the best in terms of the conversion factor. This suggests that Zn and Ti played a role as a doping ion, facilitating the isolation of charge from the photoproduced vacancy-electron pairs via a permanent electrical field [45]. The CTZ photocatalyst provided higher nitrate removal than TiO₂ and lowered the formation of nitrite and ammonia (higher selectivity), resulting in the highest total nitrogen removal with lower formic acid (highest activity). High selectivity of nitrite and low selectivity of N₂ was obtained in the first few minutes of the reaction. Nitrogen selectivity reached %90 after 20 min of reaction and then raised gradually to %95 after 60 min. The ammonia selectivity was constant entire the reaction. This means that nitrate reduction to nitrogen gas continues by the formation of nitrite. Thus initial selectivity of nitrite is high, and subsequently, nitrite ions are reduced to nitrogen gas.

TABLE 1: Selectivity to N₂ and nitrate conversion under UV irradiation^a.

	Photocatalyst	Selectivity to N ₂ [%]	Nitrate conversion [%]
1	ZnO	36.12*	33.54*
2	TiO ₂	53.44*	67.09**
3	g-C ₃ N ₄	43.67*	18.30*
4	g-C ₃ N ₄ /TiO ₂	65.34**	78.91**
5	CTZ	97.56***	95.24***
6	CTZ ^b	–	53.73*
7	CTZ ^c	97.82***	95.80***

*Being equal to 1%, **being equal to 1.5% and ***being equal to 2%.

^aConditions: NO₃⁻ (100 mL, 50 ppm), Photocatalyst (0.05 g), reaction time (60 min dark, 60 min UV irradiation), HCOOH (0.02 mol L⁻¹), UV lamp (17W, 254 nm), t = 25 °C.

^bWithout HCOOH.

^cReaction time = 120 min.

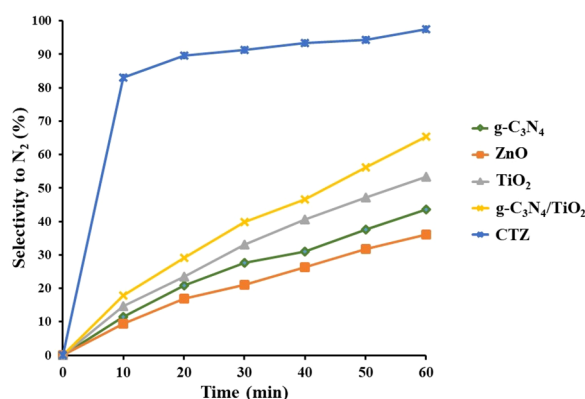


Figure 6: The N₂ selectivity for the ZnO, TiO₂, g-C₃N₄, g-C₃N₄/TiO₂, and CTZ photocatalysts.

In order to complete our experiments, nitrate removal experiments were performed under visible light irradiation, which the results were shown in Table 2. As predicted, the use of photocatalysts ZnO, TiO₂ and g-C₃N₄ in the presence of visible light irradiation is not associated with objective results (Table 2, Entries 1–3). Fortunately, the use of composite photocatalysts g-C₃N₄/TiO₂ and CTZ in these experiments yielded excellent results in nitrate reduction under visible light irradiation (Table 2, Entries 4, 5). Promising results in aqueous nitrate reduction under visible light irradiation are attributed to decrease in the nanocomposite bandgap, and thus the ease of electron–hole pair formation.

Ammonia was not produced throughout our experiments because no absorption was detected at 420 nm. No related absorption was observed in our study, and thus, we conclude that no ammonia can be produced if CTZ was used as the photocatalyst. Since nitrite and ammonia are harmful products, the significance of the present photocatalyst is its selectivity toward nitrogen gas. In terms of photocatalytic activity, the CTZ photocatalyst was the best, indicating that ZnO nanoparticles facilitate the separation of charge from the photoproduced vacancy–electron pairs via a permanent electrical field [51]. Higher nitrate removal and higher selectivity (decreased nitrite and ammonia formation) was achieved using CTZ photocatalyst compared with TiO₂, resulting in the highest total nitrogen reduction.

Reusability of the photocatalyst

The reusability of photocatalysts is an effective parameter to reduce cost of the process and the amount of waste. After each test, the photocatalyst was separated from the solution and washed three times with distilled water and dried in an oven at 90 °C for 6 h. All of the photocatalysts were reused for 6 cycles under obtained optimal conditions and the results were shown in Fig S2. Based on the obtained results, after six cycles the conversion of nitrate was 11.9%, 27.1%, 60.2%, 70.1% and 90.3% for g-C₃N₄, ZnO, TiO₂, g-C₃N₄/TiO₂, and CTZ, respectively. So,

these results showed that CTZ nanocomposite was stable and active during the photocatalytic process.

Conclusion

In this study, ZnO modified g-C₃N₄/TiO₂ photocatalyst CTZ was synthesized and characterized. The synthesis of the mesoporous and chemically stable CTZ photocatalyst with relatively high photocatalytic activity to selective nitrate reduction under UV irradiation was described here. An improved UV–visible light activity of CTZ in nitrate reduction was recorded, attributed to the synergistic effect of g-C₃N₄, ZnO, and TiO₂. The results of CTZ nanocomposite analysis using FT-IR, SEM, EDS, BET, and XRD instruments have clearly shown that the surface of the g-C₃N₄/TiO₂ is homogeneously incorporated with ZnO nanoparticles. XRD spectra confirmed the stabilization of the anatase phase by calcination at high temperatures. EDS analysis confirmed the existence of ZnO nanoparticles on the photocatalyst surfaces. The surface area of CTZ (57.04 m²/g) was enlarged significantly compared with pure g-C₃N₄ (8.21 m²/g), TiO₂ (51.27 m²/g) and ZnO (14.31 m²/g), which provided improved adsorptivity for CTZ. The UV–visible absorption increases by immobilization of the ZnO nanoparticles on the surface of the g-C₃N₄/TiO₂. Formic acid as a hole scavenger increased selectivity to nitrogen gas due to the formation of CO₂^{•-}. The photocatalyst CTZ displayed the highest nitrate photoconversion compared to other materials used in this research (95.24% in the first 60 min). The application of CTZ was associated with improved results in nitrate reduction under visible light (91.82% nitrate conversion, 95.39% N₂ selectivity). In the TiO₂/g-C₃N₄ and CTZ composites, the bandgap was lower than TiO₂ and g-C₃N₄, which facilitated the generation of photo-induced charge carriers under visible light illumination. The photocatalyst CTZ with improved photochemical properties could be further examined for possible application under solar light to remove nitrate from drinking water in industrial applications.

Materials and method

Nanocomposite characterization

The chemicals were prepared from the Merck and Fluka Companies. The functional groups of photocatalyst surfaces were determined using Fourier transform infrared spectroscopy (FT-IR; Bruker–Alpha). Field emission scanning electron microscopy (FESEM) images were captured using a Hitachi S4160 Cold Field Emission instrument. The surface elemental analysis was performed using energy-dispersive X-ray spectroscopy (EDS; SAMx). Transmission electron microscopy (TEM; Jeol JEM-1230, with an acceleration voltage of 100 kV) was performed to characterize the catalyst morphology. X-ray diffraction (XRD) was determined using a diffractometer (INEL Equinox 3000).

TABLE 2: Selectivity to N₂ and nitrate conversion under visible light irradiation^a.

	Photocatalyst	Selectivity to N ₂ [%]	Nitrate conversion [%]
1	ZnO	Trace	Trace
2	TiO ₂	Trace	Trace
3	g-C ₃ N ₄	Trace	Trace
4	g-C ₃ N ₄ /TiO ₂	71.43**	67.05**
5	CTZ	95.39***	91.82***

*Being equal to 1%, **being equal to 1.5% and ***being equal to 2%.

^aConditions: NO₃⁻ (100 mL, 50 ppm), Photocatalyst (0.05 g), reaction time (60 min visible light irradiation), HCOOH (0.02 mol L⁻¹), LED lamps (4 × 40W), *t* = 25 °C.

The specific surface areas (S_{BET}) of nanoparticles were determined by the BET method, and the pore size distributions were measured using the Barrett–Joyner–Halenda (BJH) method.

Synthesis of g-C₃N₄/TiO₂ nanocomposite

The nanocomposite g-C₃N₄/TiO₂ was synthesized similar to that described by Wang and et al. [38]. An uniform mixture of titanium dioxide (2.5 g) and melamine (2.5 g) was inserted into a crucible. It was incubated in a digital oven at 500 °C for 2 h. Finally, g-C₃N₄/TiO₂ was washed with ethanol and deionized water in an ultrasonic bath for 30 min to obtain a light yellow powder.

Synthesis of g-C₃N₄/TiO₂/ZnO nanocomposite (CTZ)

A 0.1 M solution of zinc chloride was used as the precursor for zinc oxide nanoparticles. As-prepared g-C₃N₄/TiO₂ (0.50 g) was ultrasonicated for 2 h in a precursor solution of zinc chloride (100 mL, 0.1 M) to produce a homogeneous suspension, in which Zn²⁺ ions are adsorbed uniformly onto the surface of the g-C₃N₄/TiO₂ composite. Then, an aqueous solution of NH₄HCO₃ (100 mL, 0.1 M) was added gradually into the mixture at 60 °C, and the mixture was further stirred at 60 °C for 3 h. As observed in Scheme S1, the g-C₃N₄/TiO₂ nanocomposite was prepared via a thermal approach and then ZnO nanoparticles were inserted through the g-C₃N₄/TiO₂ layers by hydrothermal approach. The obtained precipitate was filtered, washed with deionized water three times, and dried at 60 °C for 24 h. To obtain the g-C₃N₄/TiO₂/ZnO nanocomposites, the product was calcinated at 550 °C for 2 h under an N₂ atmosphere. Also, in a similar experiment for comparison, ZnO nanoparticles were prepared with the same procedure without g-C₃N₄/TiO₂.

Photocatalytic reaction conditions and calculations

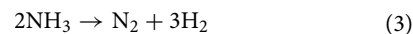
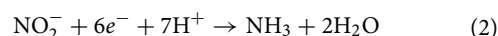
The aqueous solution containing 50 ppm NO₃⁻-N was used as the nitrate source. Photocatalytic experiments were performed in a 250 mL quartz jacketed photoreactor in a cooling tank at 25 °C and irradiated by a low-pressure Hg lamp (17 W; 254 nm) as a UV source for photocatalytic experiments and located in a double-walled quartz jacket (Scheme S2). To evaluate the photocatalytic activity under visible light irradiation, 4 LED lamps (40 W) with a total power of 160 W were used. Spectral outputs of the UV and visible light sources were illustrated in Fig. S3. The photocatalyst (50 mg) was suspended under magnetic stirring in a solution of model water (100 mL) containing 50 ppm NO₃⁻-N and formic acid (4.5 mM) as a hole scavenger. This optimum ratio of the hole scavenger concentration to the nitrate concentration was previously shown in the literature [52]. The

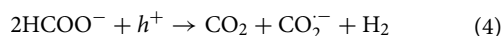
initial pH was dependent on formic acid concentration. Before irradiation by a UV lamp, the aqueous nitrate solution containing the photocatalyst was stirred in the dark for 1 h to determine the adsorption rate of the photocatalyst to study the non-photocatalytic removal. The total duration for irradiation with UVC light was 60 min.

A set of parallel experiments were performed without nitrate, hole scavenger, irradiation, photocatalyst, respectively. During the experiments, samples were withdrawn every 10 min. At the end of the reaction, the photocatalyst was immediately removed from the solution by centrifugation, and the filtrate was analyzed to determine the residual concentration of nitrate. To evaluate the adequate conditions, experiments were carried out by varying the photocatalyst amount and UV irradiation, keeping the concentration of nitrate constant (50 mg L⁻¹) under the experimental conditions. Experiments were also carried out using various photocatalyst dosages to determine the impact of photocatalyst concentration on nitrate removal, keeping the other parameters constant under the experimental conditions. Different photocatalytic systems previously prepared were performed applying the above conditions. To determine the actual effect of the photocatalytic systems, experiments were conducted with ZnO, TiO₂, g-C₃N₄, g-C₃N₄/TiO₂, and g-C₃N₄/TiO₂/ZnO under UV irradiation and visible light irradiation, respectively.

Analytical methods for the determination of nitrogen compounds

After photocatalytic reactions, samples were analyzed for nitrate, nitrite, and ammonia concentrations. Nitrate and nitrite anions were measured using a UV–Vis spectrophotometer operated at 220 and 275 nm, respectively. The concentration of ammonia and total dissolved nitrogen (TDN) were determined using colorimetric methods (Hach DR2000 UV–VIS, Kit #TNT827, and Hach DR2000 UV–VIS, Kit #TNT830, respectively). The samples were analyzed after collection to determine the pH and concentrations of nitrate (NO₃⁻), nitrite (NO₂⁻), ammonium (NH₄⁺), TOC, and TDN. The initial pH was about 2.5 because of the addition of formic acid, which slowly increased and reached 3.5 after 60 min due to acid consumption. Nitrate ions may be photocatalytically reduced to generate ammonia (Eqs. 1, 2), which would then be decomposed to form hydrogen and nitrogen (Eq. 3) [53]. Formic acid appears as a hole scavenger and produces gaseous carbon dioxide, anion radical carbon dioxide, and hydrogen (Eq. 4).





The selectivity to N_2 and nitrate conversion were evaluated using Eqs. 5 and 6, respectively [54]. The most effective photocatalyst is that achieved the highest mentioned values. Nitrogen selectivity is described as the ratio between nitrate concentrations reduced to nitrogen and total nitrate concentration reduced, assuming no by-products are produced other than NO_2^- and NH_3 .

$$\begin{aligned} \text{Selectivity to } \text{N}_2(\%) &= \frac{N_{2,\text{formed}}}{[\text{NO}_3^- - N]_{\text{reduced}}} \times 100 \\ &= \frac{(NT_i - NT_t)}{[\text{NO}_3^- - N]_i - [\text{NO}_3^- - N]_t} \quad (5) \end{aligned}$$

$$\text{Nitrate conversion}(\%) = \frac{[\text{NO}_3^- - N]_i - [\text{NO}_3^- - N]_t}{[\text{NO}_3^- - N]_i} \times 100 \quad (6)$$

where i is initial concentration, t is concentration at time t and $(\text{NO}_3^- - \text{N})$ is nitrogen present as nitrate.

Acknowledgments

The authors appreciate ACECR—Tehran Organization, Kharazmi University and Shahid Chamran University of Ahvaz for all their support.

Author contributions

Mohammad Hadi Ghasemi: Investigation, Methodology, Writing—original draft. Reyhaneh Kaveh: Investigation, Methodology, Supervision, Writing—review & editing. Hassan Alijani: Investigation, Methodology. Elham Asadi: Investigation. Elaheh Bohloulbandi: Investigation. Majid Baghdadi: Investigation.

Funding

No funding was received for conducting this study.

Data availability

Data will be made available on reasonable request.

Declarations

Conflict of interest The authors declare that they have no known competing financial interests or personal relationships that could have appeared to influence the work reported in this paper.

Supplementary Information

The online version contains supplementary material available at <https://doi.org/10.1557/s43578-024-01292-x>.

References

1. U. Baig, M. Faizan, M. Sajid, Effective removal of hazardous pollutants from water and deactivation of water-borne pathogens using multifunctional synthetic adsorbent materials: a review. *J. Clean. Prod.* **302**, 126735 (2021). <https://doi.org/10.1016/j.jclepro.2021.126735>
2. S. Li, M. Cai, Y. Liu, C. Wang, R. Yan, X. Chen, Constructing $\text{Cd}_{0.5}\text{Zn}_{0.5}\text{S}/\text{Bi}_2\text{WO}_6$ S-scheme heterojunction for boosted photocatalytic antibiotic oxidation and Cr(VI) reduction. *Adv. Powder Mater.* **2**(1), 100073 (2023). <https://doi.org/10.1016/j.apmate.2022.100073>
3. M. Cai, Y. Liu, C. Wang, W. Lin, S. Li, Novel $\text{Cd}_{0.5}\text{Zn}_{0.5}\text{S}/\text{Bi}_2\text{MoO}_6$ S-scheme heterojunction for boosting the photodegradation of antibiotic enrofloxacin: degradation pathway, mechanism and toxicity assessment. *Sep. Purif. Technol.* **304**, 122401 (2023). <https://doi.org/10.1016/j.seppur.2022.122401>
4. A. Vahid, M. Abdouss, S. Nayeri, A. Miran Beigi, Simultaneous adsorption of cationic and anionic dyes using a novel multifunctional mesoporous silica. *Anal. Method Environ. Chem. J.* **4**(1), 46–57 (2021). <https://doi.org/10.24200/amecj.v4.i01.127>
5. S. Li, R. Yan, M. Cai, W. Jiang, M. Zhang, X. Li, Enhanced antibiotic degradation performance of $\text{Cd}_{0.5}\text{Zn}_{0.5}\text{S}/\text{Bi}_2\text{MoO}_6$ S-scheme photocatalyst by carbon dot modification. *J. Mater. Sci. Technol.* **164**, 59–67 (2023). <https://doi.org/10.1016/j.jmst.2023.05.009>
6. S. Li, C. Wang, K. Dong, P. Zhang, X. Chen, X. Li, MIL-101 (Fe)/BiOBr S-scheme photocatalyst for promoting photocatalytic abatement of Cr (VI) and enrofloxacin antibiotic: performance and mechanism. *Chin. J. Catal.* **51**, 101–112 (2023). [https://doi.org/10.1016/S1872-2067\(23\)64479-1](https://doi.org/10.1016/S1872-2067(23)64479-1)
7. S. Li, M. Cai, C. Wang, Y. Liu, $\text{Ta}_3\text{N}_5/\text{CdS}$ core–shell S-scheme heterojunction nanofibers for efficient photocatalytic removal of antibiotic tetracycline and Cr (VI): performance and mechanism insights. *Adv. Fiber Mater.* **5**, 994–1007 (2023). <https://doi.org/10.1007/s42765-022-00253-5>
8. C. Wang, R. Yan, M. Cai, Y. Liu, S. Li, A novel organic/inorganic S-scheme heterostructure of TCPP/ $\text{Bi}_{12}\text{O}_{17}\text{Cl}_{12}$ for boosting photodegradation of tetracycline hydrochloride: kinetic, degradation mechanism, and toxic assessment. *Appl. Surf. Sci.* **610**, 155346 (2023). <https://doi.org/10.1016/j.apsusc.2022.155346>
9. C.A. Grande, R. Blom, V. Middelkoop, D. Matras, A. Vamvakeros, S.D. Jacques, A.M. Bouzga, Multiscale investigation of adsorption properties of novel 3D printed UTSA-16 structures. *Chem. Eng. J.* **402**, 12616 (2020). <https://doi.org/10.1016/j.cej.2020.126166>
10. S. Li, M. Cai, Y. Liu, C. Wang, K. Lv, X. Chen, S-Scheme photocatalyst TaON/ Bi_2WO_6 nanofibers with oxygen vacancies for efficient abatement of antibiotics and Cr (VI): intermediate eco-toxicity analysis and mechanistic insights. *Chin. J. Catal.* **43**, 2652–2664 (2022). [https://doi.org/10.1016/S1872-2067\(22\)64106-8](https://doi.org/10.1016/S1872-2067(22)64106-8)

11. M. Cai, Y. Liu, K. Dong, X. Chen, S. Li, Floatable S-scheme Bi₂WO₆/C₃N₄/carbon fiber cloth composite photocatalyst for efficient water decontamination. *Chin. J. Catal.* **52**, 239–251 (2023). [https://doi.org/10.1016/S1872-2067\(23\)64496-1](https://doi.org/10.1016/S1872-2067(23)64496-1)
12. G. Liu, Y. Zhou, Z. Liu, J. Zhang, B. Tang, S. Yang, C. Sun, Efficient nitrate removal using micro-electrolysis with zero valent iron/activated carbon nanocomposite. *J. Chem. Technol. Biotechnol.* **91**, 2942–2949 (2016). <https://doi.org/10.1002/jctb.4910>
13. H.O.N. Tugaoen, P. Herckes, P. Westerhoff, Influence of ultra-violet wavelengths on kinetics and selectivity for N-gases during TiO₂ photocatalytic reduction of nitrate. *Appl. Catal. B* **220**, 597–606 (2018). <https://doi.org/10.1016/j.apcatb.2017.08.078>
14. M.J. Kim, S.S. Choi, P.B.S. Rallapalli, H.J. Ha, S. Lee, Y. Lee, Nitrate removal from water phase using Robinia pseudoacacia bark for solving eutrophication. *Korean J. Chem. Eng.* **36**, 1450–1454 (2019). <https://doi.org/10.1007/s11814-019-0331-x>
15. P. Yoo, Y. Amano, M. Machida, Adsorption of nitrate onto nitrogen-doped activated carbon fibers prepared by chemical vapor deposition. *Korean J. Chem. Eng.* **35**, 2468–2473 (2018). <https://doi.org/10.1007/s11814-018-0151-4>
16. L.M. Wild, B. Mayer, F. Einsiedl, Decadal delays in groundwater recovery from nitrate contamination caused by low O₂ reduction rates. *Water Resour. Res.* **54**, 9996–10012 (2018). <https://doi.org/10.1029/2018WR023396>
17. B. Wang, S.Y. Liu, F.Y. Li, Z. Fan, Removal of nitrate from constructed wetland in winter in high-latitude areas with modified hydrophyte biochars. *Korean J. Chem. Eng.* **34**, 717–722 (2017). <https://doi.org/10.1007/s11814-016-0308-y>
18. L. Zhu, X. Zhu, C. Zhang, T. Huo, X. Hou, D. Guo, H. Zhang, D. Xia, Enhanced visible-light catalytic degradation of methylene blue by improving adsorption of porous zirconium-based porphyrin MOFs sensitized TiO₂ photocatalyst. *J. Mater. Res.* **36**, 2961–2972 (2021). <https://doi.org/10.1557/s43578-021-00303-5>
19. J. Hirayama, R. Abe, Y. Kamiya, Combinational effect of Pt/SrTiO₃:Rh photocatalyst and SnPd/A₁2O₃ non-photocatalyst for photocatalytic reduction of nitrate to nitrogen in water under visible light irradiation. *Appl. Catal. B* **144**, 721–729 (2014). <https://doi.org/10.1016/j.apcatb.2013.08.005>
20. Y. Li, S.G. Li, J. Wang, C.H. Ma, L. Zhang, Preparation and solar-light photocatalytic activity of TiO₂ nanocomposites: TiO₂/kaolin, TiO₂/diatomite, and TiO₂/zeolite. *Russ. J. Phys. Chem. A* **88**, 2471–2475 (2014). <https://doi.org/10.1134/S0036024414130123>
21. R. Kaveh, M. Mokhtarifar, M. Bagherzadeh, A. Lucotti, M.V. Diamanti, M.P. Pedferri, Magnetically recoverable TiO₂/SiO₂/γ-Fe₂O₃/rGO composite with significantly enhanced UV-visible light photocatalytic activity. *Molecules* **25**, 2996 (2020). <https://doi.org/10.3390/molecules25132996>
22. S. Jayapandi, P. Backialakshmi, P. Soundarrajan, M. Senthil Pandian, P. Ramasamy, S. Suresh Kumar, C. Gopinathan, Construction of p–n junction type Ag₂O/SnO₂ heterostructure photocatalyst for enhanced organic dye degradation under direct sunlight irradiation: experimental and theoretical investigations. *J. Mater. Res.* **38**, 753–766 (2023). <https://doi.org/10.3390/molecules25132996>
23. M. Mokhtarifar, D.T. Nguyen, M.V. Diamanti, R. Kaveh, M. Asa, M. Sakar, M.P. Pedferrib, T.O. Do, Fabrication of dual-phase TiO₂/WO₃ with post-illumination photocatalytic memory. *N. J. Chem.* **44**, 20375–20386 (2020). <https://doi.org/10.1039/D0N104694A>
24. Y. Sakatani, H. Ando, K. Okusako, H. Koike, J. Nunoshige, T. Takata, J.N. Kondo, H. Domen, Metal ion and N co-doped TiO₂ as a visible-light photocatalyst. *J. Mater. Res.* **19**, 2100–2108 (2004). <https://doi.org/10.1557/JMR.2004.0269>
25. M. Huang, J. Li, M. Wu, H. Wang, M. Fan, W. Huang, L. Dong, B. Li, Enhanced visible light absorption CdS-decorated direct Z-scheme g-C₃N₄/TiO₂ for improved photocatalysis and hydrogen generation. *J. Mater. Res.* **37**, 2241–2256 (2022). <https://doi.org/10.1557/s43578-022-00614-1>
26. P. Zhou, J. Yu, Y. Wang, The new understanding on photocatalytic mechanism of visible-light response N-S codoped anatase TiO₂ by first-principles. *Appl. Catal. B* **142–143**, 45–53 (2013). <https://doi.org/10.1016/j.apcatb.2013.04.063>
27. K. Dai, L.H. Lu, C.H. Liang, Q. Liu, G.P. Zhu, Heterojunction of facet coupled g-C₃N₄/surface-fluorinated TiO₂ nanosheets for organic pollutants degradation under visible LED light irradiation. *Appl. Catal. B* **156–157**, 331–340 (2014). <https://doi.org/10.1016/j.apcatb.2014.03.039>
28. A.Y. Yan, A.H. Yang, B.Z. Yi, A.R. Li, T. Xian, Design of ternary CaTiO₃/g-C₃N₄/AgBr Z-scheme heterostructured photocatalysts and their application for dye photodegradation. *Solid State Sci.* **100**, 106102 (2020). <https://doi.org/10.1016/j.solidstatesciences.2019.106102>
29. Q. Shen, C. Wu, Z. You, F. Huang, J. Sheng, F. Zhang, D. Cheng, H. Yang, g-C₃N₄ nanoparticle@porous g-C₃N₄ composite photocatalytic materials with significantly enhanced photo-generated carrier separation efficiency. *J. Mater. Res.* **35**, 2148–2157 (2020). <https://doi.org/10.1557/jmr.2020.182>
30. Y. Wang, X. Wang, M. Antonietti, Polymeric graphitic carbon nitride as a heterogeneous organocatalyst: from photochemistry to multipurpose catalysis to sustainable chemistry. *Angew. Chem. Int. Ed.* **51**, 68–89 (2012). <https://doi.org/10.1002/anie.201101182>
31. D. Mitoraj, H. Kisch, The nature of nitrogen-modified titanium dioxide photocatalysts active in visible light. *Angew. Chem. Int. Ed.* **47**, 9975–9978 (2008). <https://doi.org/10.1002/anie.200800304>

32. L.A. Al-Hajji, A.A. Ismail, M.F. Atitar, I. Abdelfattah, A.M. El-Toni, Construction of mesoporous g-C₃N₄/TiO₂ nanocrystals with enhanced photonic efficiency. *Ceram. Int.* **45**, 1265–1272 (2019). <https://doi.org/10.1016/j.ceramint.2018.10.009>
33. A. Sudhaik, P. Raizada, P. Shandilya, D.Y. Jeong, J.H. Lim, P. Singh, Review on fabrication of graphitic carbon nitride based efficient nanocomposites for photodegradation of aqueous phase organic pollutants. *J. Ind. Eng. Chem.* **67**, 28–51 (2018). <https://doi.org/10.1016/j.jiec.2018.07.007>
34. Y. Zou, J.W. Shi, D. Ma, Z. Fan, L. Lu, C. Niu, In situ synthesis of C-doped TiO₂@g-C₃N₄ core-shell hollow nanospheres with enhanced visible-light photocatalytic activity for H₂ evolution. *Chem. Eng. J.* **322**, 435–444 (2017). <https://doi.org/10.1016/j.cej.2017.04.056>
35. M.A. Karimi, M.H. Ghasemi, M.J. Aghagoli, M.H. Beyki, Pre-concentration of cobalt ions by a melamine-modified cellulose@MWCNT nanohybrid. *Mikrochim. Acta* **183**, 2949–2955 (2016). <https://doi.org/10.1007/s00604-016-1943-z>
36. M.H. Beyki, H. Alijani, M.H. Ghasemi, Melamine-anchored magnetic multiwall carbon nanotubes: tailoring functional groups reactivity for efficient adsorption of anionic dye. *Desalin. Water Treat.* **57**, 20565–20573 (2016). <https://doi.org/10.1080/19443994.2015.1109559>
37. D. Jiang, H. Yu, H. Yu, Modified g-C₃N₄/TiO₂ nanosheets/ZnO ternary facet coupled heterojunction for photocatalytic degradation of p-toluenesulfonic acid (p-TSA) under visible light. *Physica E* **85**, 1–6 (2017). <https://doi.org/10.1016/j.physe.2016.08.014>
38. J. Wang, J. Huang, H. Xie, A. Qu, Synthesis of g-C₃N₄/TiO₂ with enhanced photocatalytic activity for H₂ evolution by a simple method. *Int. J. Hydrog. Energy* **39**, 6354–6363 (2014). <https://doi.org/10.1016/j.ijhydene.2014.02.020>
39. R. Wahab, S.G. Ansari, Y.S. Kim, H.K. Seo, G.S. Kim, G. Khang, H.S. Shin, Low temperature solution synthesis and characterization of ZnO nano-flowers. *Mater. Res. Bull.* **42**, 1640–1648 (2007). <https://doi.org/10.1016/j.materresbull.2006.11.035>
40. G. Nagaraju, Udayabhanu, S.A. Prashanth, M. Shastri, K.V. Yathish, C. Anupama, Electrochemical heavy metal detection, photocatalytic, photoluminescence, biodiesel production and antibacterial activities of Ag-ZnO nanomaterial. *Mater. Res. Bull.* **94**, 54–63 (2017). <https://doi.org/10.1016/j.materresbull.2017.05.043>
41. J. Li, Y. Liu, H. Li, C. Chen, Fabrication of g-C₃N₄/TiO₂ composite photocatalyst with extended absorption wavelength range and enhanced photocatalytic performance. *J. Photochem. Photobiol. A* **317**, 151–160 (2016). <https://doi.org/10.1016/j.jphotochem.2015.11.008>
42. M. Troppová, M. Šihor, M. Reli, P. Ritz, K. Praus, Kočí, Unconventionally prepared g-C₃N₄/TiO₂ photocatalysts for photocatalytic decomposition of nitrous oxide. *Appl. Surf. Sci.* **430**, 335–347 (2018). <https://doi.org/10.1016/j.apsusc.2017.06.299>
43. M. Davarpanah, A. Ahmadpour, T. Rohani-Bastami, H. Dabir, Synthesis and application of diethanolamine-functionalized polystyrene as a new sorbent for the removal of p-toluenesulfonic acid from aqueous solution. *J. Ind. Eng. Chem.* **30**, 281–288 (2015). <https://doi.org/10.1016/j.jiec.2015.05.034>
44. M. Mokhtarifar, R. Kaveh, M. Bagherzadeh, A. Lucotti, M.P. Pedferri, M.V. Diamanti, Heterostructured TiO₂/SiO₂/γ-Fe₂O₃/rGO coating with highly efficient visible-light-induced self-cleaning properties for metallic artifacts. *ACS Appl. Mater. Interfaces* **12**, 29671–29683 (2020). <https://doi.org/10.1021/acsami.0c06792>
45. M.R. Arefi, S. Rezaei-Zarchi, Synthesis of zinc oxide nanoparticles and their effect on the compressive strength and setting time of self-compacted concrete paste as cementitious composites. *Int. J. Mol. Sci.* **13**, 4340–4350 (2012). <https://doi.org/10.3390/ijms13044340>
46. T. Yang, S. Park, T. Gon Kim, D.S. Shin, K. Suh, J. Park, Ultra-violet photodetector using pn junction formed by transferrable hollow n-TiO₂ nano-spheres monolayer. *Opt. Express* **25**, 30843–30850 (2017). <https://doi.org/10.1364/OE.25.030843>
47. S. Bagheri, K. Shamel, S. B. A. Hamid, Synthesis and characterization of anatase titanium dioxide nanoparticles using egg white solution via sol-gel method. *J. Chem.* **2013**, 848205 (2012). <https://doi.org/10.1155/2013/848205>
48. A. Kumar, P. Kumar, C. Joshi, M. Manchanda, R. Boukherroub, S.L. Jain, Nickel decorated on phosphorous-doped carbon nitride as an efficient photocatalyst for reduction of nitrobenzenes. *Nanomaterials* **6**, 59–73 (2016). <https://doi.org/10.3390/nano6040059>
49. R.A. Senthil, J. Theerthagiri, A. Selvi, J. Madhavan, Synthesis and characterization of low-cost g-C₃N₄/TiO₂ composite with enhanced photocatalytic performance under visible-light irradiation. *Opt. Mater.* **64**, 533–539 (2017). <https://doi.org/10.1016/j.optmat.2017.01.025>
50. H. Alijani, R. Kaveh, Preparation of rGO-CNT/Ag₃PO₄/Nb₂O₅ composite with enhanced photoresponse properties as a highly effective visible light driven photocatalyst. *J. Chem. Technol. Biotechnol.* (2022). <https://doi.org/10.1002/jctb.7151>
51. L. Pan, G.Q. Shen, J.W. Zhang, X.C. Wei, L. Wang, J.J. Zou, X. Zhang, TiO₂-ZnO composite sphere decorated with ZnO clusters for effective charge isolation in photocatalysis. *Ind. Eng. Chem. Res.* **54**, 7226–7232 (2015). <https://doi.org/10.1021/acs.iecr.5b01471>
52. F. Zhang, R. Jin, J. Chen, C. Shao, W. Gao, L. Li, N. Guan, High photocatalytic activity and selectivity for nitrogen in nitrate reduction on Ag/TiO₂ catalyst with fine silver clusters. *J. Catal.* **32**, 424–431 (2005). <https://doi.org/10.1016/j.jcat.2005.04.014>

53. S. Rengaraj, X.Z. Li, Enhanced photocatalytic reduction reaction over Bi^{3+} - TiO_2 nanoparticles in presence of formic acid as a hole scavenger. *Chemosphere* **66**, 930–938 (2007). <https://doi.org/10.1016/j.chemosphere.2006.06.007>
54. D.D.B. Luiz, S.L.F. Andersen, C. Berger, H.J. José, Moreira RDFPM, Photocatalytic reduction of nitrate ions in water over metal-modified TiO_2 . *J. Photochem. Photobiol. A* **246**, 36–44 (2012). <https://doi.org/10.1016/j.jphotochem.2012.07.011>

Publisher's Note Springer Nature remains neutral with regard to jurisdictional claims in published maps and institutional affiliations.

Springer Nature or its licensor (e.g. a society or other partner) holds exclusive rights to this article under a publishing agreement with the author(s) or other rightsholder(s); author self-archiving of the accepted manuscript version of this article is solely governed by the terms of such publishing agreement and applicable law.